JOURNAL OF APPLIED ENGINEERING SCIENCES
ISSN: 2247-3769 / e-ISSN: 2284-7197

sciendo

VOL. 15(28), ISSUE 2/2025
ART.NO. 459 pp. 243-250

CYCLIC LOADING-INDUCED SURFACE DEGRADATION AND ITS EFFECT ON THE FRICTIONAL BEHAVIOR OF TIRE-ASPHALT CONTACT

S.R La [a,b], X.B Li [c,d,*], Anhua Xu [e], J.H Fang [b]

[a.] School of Civil and Transportation Engineering, Qinghai Minzu University, Xining, Qinghai 810007, China, E-mail: 837848924@qq.com
[b] Qinghai Research Institute of Transportation, Xining, Qinghai 810016, China, E-mail: 1007361863@qq.com
[c*] School of Civil Engineering, Chongqing University, Chongqing 400045, China / [d] Qinghai Lake Tourism Development Group Co., Ltd., Qinghai Province, Xining, Qinghai 810007, China, E-mail: qhjiaotongkeji@163.com
[e] Qinghai Vocational and Technical University, Xining, Qinghai 810016, China, E-mail: 347024683@qq.com

Received: 17.06.2025 / Accepted: 21.07.2025 / Revised: 08.10.2025 / Available online: 15.12.2025

DOI: 10.2478/jaes-2025-0029

KEY WORDS: Tire Asphalt Pavement, Surface Roughness, Cyclic Loading, Discrete Particles, Elastic Contact Model.

ABSTRACT:

This study investigates the cyclic friction properties of asphalt pavements under repeated loading by developing a custom-designed testing apparatus, which was rigorously calibrated to ensure stability and experimental reliability. Results show that both the frictional force and surface roughness decrease with increasing cycles, exhibiting a clear linear correlation. SEM analysis reveals the formation and accumulation of discrete abrasive particles on the tire surface, identified as a key factor contributing to frictional instability. Based on elastoplastic contact theory, the reduction in surface roughness is attributed to stress concentrations at the boundary layer, leading to material removal and wear particle generation. Furthermore, a spring-slider numerical model was established, and its initial results qualitatively match experimental findings. By adjusting the roughness parameter, the model demonstrates that friction force gradually decreases and stick-slip behavior weakens with increasing cycles, consistent with the experimental trends.

1. INTRODUCTION

Asphalt pavement, which forms the main structural layer of highways, is subjected to continuous repetitions of traffic loading as well as environmental actions (Fwa, 2017; Liu et al., 2023; Sara et al., 2021). Among its functional attributes, skid resistance is a key determinant of driving safety and thus serves as an essential criterion in pavement construction and maintenance practices (Mahajan et al., 2022; Wei et al., 2023). Fundamentally, pavement skid resistance characterizes the vehicle's braking capability, governed by the frictional forces generated at the tire–pavement interface. These forces depend strongly on the pavement surface features, particularly its texture and roughness. To address research demands related to tire–road friction behavior, a variety of skid-resistance testing devices have been developed. Most operate based on dynamic sliding contact between a rubber slider and the pavement, from which the resisting torque of the slider is recorded and subsequently converted into a friction coefficient. According to testing mode, these devices can be categorized into single-point and continuous-measurement systems. For instance, Tan et al. (2019) examined the skid behavior of rubber sliders on icy surfaces using the Dynamic Friction Tester (DFT). In practical applications, the pavement friction coefficient is widely used as a key indicator in accident analysis and forensic investigations (Beketov, Khalimova, 2023; Roy et al., 2023). As a classical assessment parameter, it has been extensively adopted in skid-resistance studies (Luo et al., 2024; Rith et al., 2020). Representative single-point devices include the pendulum friction tester (Qian, Meng, 2017) and the dynamic friction tester (Chu et al., 2019), while continuous-measurement equipment comprises locked-wheel friction testing vehicles (Yu et al., 2020), SCRIM lateral-force testing vehicles (Sajid et al., 2021), and other friction-meter systems (He et al., 2023). In recent work, Novikov and Lazarev (2017) incorporated factors such as vehicle speed, axle load, braking distance, and tire pressure into skid-testing research and developed a variable-parameter apparatus capable of evaluating friction coefficients under various braking and lateral-slip conditions. Hofko et al. (2019) engineered the Road Star testing vehicle, designed with an 18% slip rate, and achieved high-resolution in-situ skid measurements; its results showed strong consistency with the Wehner/Schulze laboratory test (R^2 = 0.89), independent of pavement type.

[*] Corresponding author: Xiaobin Li, Professor, School of Civil Engineering, Chongqing University, Chongqing 400045, China; Qinghai Lake Tourism Development Group Co., Ltd., Xining, Qinghai 810007, China. E-mail: qhjiaotongkeji@163.com.

Additionally, Gerardo et al. (2018) compared three friction-testing devices—LWST (with treaded and smooth tires), Grip Tester, and SCRIM—using orthogonal regression, and demonstrated that SCRIM exhibited strong correlation with LWST treaded-tire results, whereas the Grip Tester correlated more closely with LWST smooth-tire measurements.

From the perspective of theoretical analysis and numerical simulation, Adamcs (2012) explored the mechanisms governing tire–pavement friction and pointed out that the total friction force arises from the combined contributions of adhesion and hysteretic deformation of rubber on rough surfaces. Tomaraee et al. (2015) extracted geometric characteristics of tire contact patches from processed images and experimentally investigated how the contact length and width vary with vertical load and inflation pressure, thereby revealing their influence on rolling resistance. Juan (2017) developed a non-contact measurement system for tire contact pressure and experimentally examined how load, inflation pressure, and camber angle affect the spatial distribution of contact stress. Long-term monitoring by Georgouli et al. (2016) demonstrated a clear seasonal pattern in pavement skid resistance, with both friction force and coefficient reaching maximum values during low-temperature winter periods and minimum values during summer. Using dynamic loading simulations, Lin et al. (2018) analyzed the influence of fine aggregate angularity on the skid resistance of asphalt pavements, employing pendulum friction values and texture depth as performance indicators after specified load repetitions. Guo (2016) introduced a tire adhesion coefficient testing method based on a newly constructed test rig, obtained the evolution of friction factor with slip ratio, refined an existing semi-empirical steady-state sideslip model, and proposed a unified semi-empirical formulation combining brush-type models with measured data. Kane and Edmondson (2022) treated tire rubber as a viscoelastic medium, formulated a simplified viscoelastic–rough surface contact model, and applied it to predict tire–road friction. Considering rubber viscoelasticity, Ciavarella (2017) further simplified Persson's multi-scale friction theory, arguing that highly rough asphalt surfaces can be approximated by a single-scale model when the wave vector reaches extreme values, with a fractal dimension around $D \approx 2.2$, and validated the simplification through comparisons with Lorenz-based calculations. In tire–road contact modeling, Wang et al. (2015) constructed a three-dimensional nonlinear tire finite element model in ABAQUS to describe the load–deformation relationship, while Gupta et al. (2020) employed ANSYS to investigate the static response of inflated rubber tires in contact with steel rails. Serigos et al. (2016) assessed pavement surface texture and established a predictive relationship between texture characteristics and frictional performance, showing a notable correlation with BPN values. Liu et al. (2023) applied the discrete element method to build an asphalt pavement model under wheel loading and conducted dynamic response analysis. In studies of pavement dynamic loading, researchers have also shown that a linear combination of multiple half-sine pulses can approximate nonlinear load variations induced by surface irregularities. Furthermore, due to the viscoelastic behavior of asphalt materials, a half-sine load with an appropriate recovery period can represent the transient and impact characteristics of pavement loading (Krishnanunni, Rao, 2019; Yan et al., 2019). To support surface characterization, Behrouz et al. (2022) designed a three-dimensional texture measurement system using cumulative imaging and Structure-from-Motion (SfM), achieving efficient and accurate point-cloud reconstruction with simplified operation.

Despite notable advances in understanding asphalt pavement friction over recent years, the evolution of frictional behavior under repeated loading has remained insufficiently explored, largely due to constraints in existing testing technologies. To address this gap, this study designs and constructs a specialized apparatus capable of evaluating tire–asphalt friction characteristics under cyclic loading conditions. Using this device, the wear behavior of both tires and asphalt surfaces under repeated loads and the influence of detached particles are systematically examined. Furthermore, based on elastic contact theory, the study elucidates the evolution mechanism of friction during cyclic loading, providing new insights into the dynamic frictional response of asphalt pavements.

2. TESTING DEVICE AND STABILITY ANALYSIS

To meet the experimental requirements for evaluating tire–asphalt friction under cyclic loading, a dedicated testing apparatus was independently designed and fabricated in this study, as shown in Figure 1(a) and 1(b). The setup comprises a material testing machine, a high-precision strain acquisition instrument, a fixed pulley, thermocouples, a counterweight, and other components. Among them, the high-precision strain acquisition instrument is a key electronic device designed to monitor and record the force variations experienced by strain sensors in real time. It amplifies, filters, and digitizes the minute voltage signals generated by the strain sensors, allowing for accurate strain measurement and subsequent conversion into frictional force values. With its high accuracy and rapid response speed, the instrument meets the stringent demands for evaluating tire-asphalt friction performance under complex loading conditions. The material testing machine is used to provide a stable tensile force and precisely control the stretching rate, thereby simulating the relative sliding between the tire and asphalt surface at different velocities. The fixed pulley is incorporated to redirect the force direction, enabling planar friction between the asphalt specimen and the sliding block; its design ensures stable and accurate force transmission while minimizing errors due to directional shifts. Additionally, a traction line made of highly elastic material.

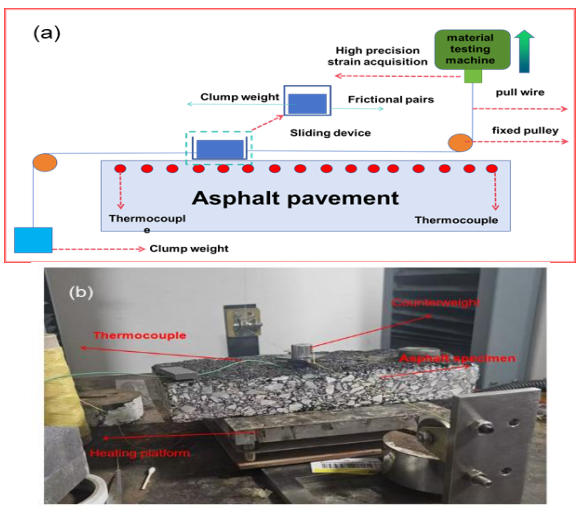

Figure 1. (a) Schematic and (b) experimental setup for the cyclic friction performance of tire-asphalt pavement

The device captures the voltage signal produced by the relative sliding between the tire and the asphalt pavement using high-precision sensors, and subsequently derives the frictional force through a calibration process. The calibration procedure involves suspending various standard masses from the strain sensor to obtain corresponding voltage readings, establishing a relationship to calibrate the strain acquisition instrument. Figure 2 demonstrates that the voltage responses associated with the four standard masses maintain a highly linear relationship. The resulting force resolution of 0.1 mN is sufficient for characterizing tire–asphalt pavement friction. The apparatus employs a highly elastic traction wire to connect the slider to a high-precision sensor, thereby mitigating the impact of traction wire deformation on the test data.

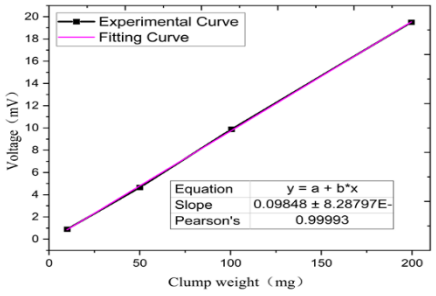

Figure 2. Voltage variation curve in relation to counterweight mass

This device utilizes a fixed pulley transmission system to facilitate planar friction between the asphalt pavement and the sliding block. Figure 3(a) illustrates the schematic of the traction-line–pulley testing setup, and Figure 3(b) presents the corresponding friction force curve. As shown, the friction force generated between the traction line and the pulley remains below 0.6 mV and exhibits a stable response throughout the test. Consequently, the testing device is capable of assessing the frictional characteristics of asphalt pavements and meets the necessary testing criteria.

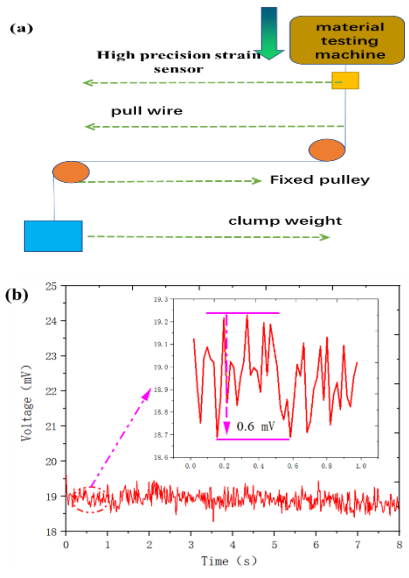

Figure 3. (a) Schematic of the frictional interaction between the traction wire and pulley; (b) Corresponding friction force curve for the traction wire–pulley system.

3. EXPERIMENTAL TESTS

3.1. Impact of cyclic loading on tire surface roughness

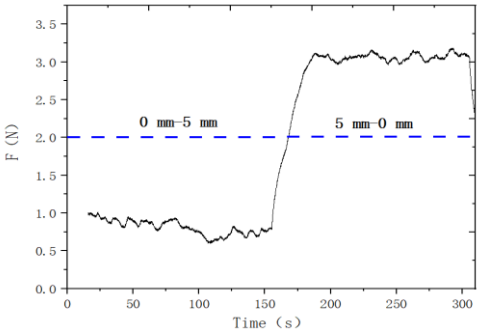

Figure 4. Time-dependent profile of frictional force during a single loading cycle

This study employs custom-designed apparatus to examine the surface roughness of tire asphalt pavement subjected to cyclic loading. The asphalt type chosen for the experiments is AC-13 grade, with a bitumen-to-aggregate ratio of 5.0 %. A smooth rubber tire, measuring 5 mm by 5 mm, serves as the frictional counterpart. The tire slider's surface roughness is adjustable, achieved through the application of various grades of sandpaper for polishing. The loading speed is set at 2 mm/min, with a 200 g weight applied. The environmental temperature is maintained at 23°C. The loading trajectory consists of a single path from 0 mm to 5 mm and back to 0 mm, with the entire cycle of loading lasting 300 seconds, as depicted in Figure 4.

The surface roughness of tires at a specific location is evaluated using a Laser Check 6212 contact roughness meter (Schmidt Industries), as depicted in Figure 5. The average roughness starts at Ra = 3.8 µm after the first cycle, declines to Ra = 3.23 µm after 10 cycles, and reaches Ra = 2.96 µm after 20 cycles. The comparison of data shows that as the number of cycles increases, the tire surface's average roughness gradually decreases, along with a decline in vibration amplitude.

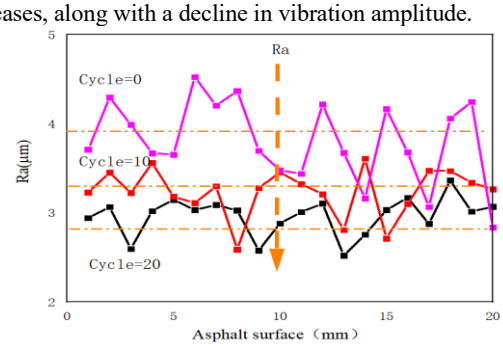

Figure 5. Variation in surface roughness with increasing cycle durations

3.2. Impact of cycle count on the frictional properties of asphalt pavements

As depicted in Figure 6, the frictional force changes over time with increasing cycle numbers. The figure reveals that the average friction force during the initial cycle is 3.05 N, which slightly decreases to 3.02 N after 5 cycles, to 3.00 N after 10 cycles, and to 2.98 N following 20 cycles. The results show that the relative sliding friction between the tire and asphalt

pavement decreases with an increasing number of cycles. A comparison of the friction force curves in regions I, II, and III, under 1 and 5 cycles, shows that the friction force curve becomes progressively flatter with an increase in cycle count. When comparing the friction force curves at 5 and 10 cycles, a significant elongation of the complete viscous (H) to slip (L) transition is observed, along with pronounced fluctuations in the friction force curve, as depicted in Figure 5(c). A comparison of the friction force curves at 10 and 20 cycles reveals a noticeable reduction in vibration amplitude, accompanied by a decrease in the average friction force.

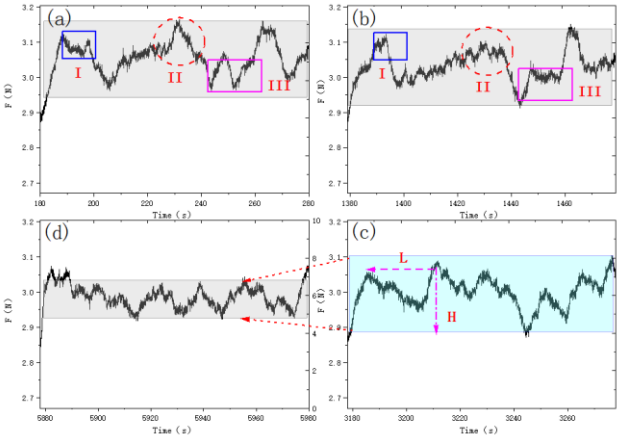

Figure 6. Temporal variation of friction force under varying cycle counts: (a) 1 cycle; (b) 5 cycles; (c) 10 cycles; (d) 20 cycles

3.3. Influence of discrete particles on cyclic friction characteristics

SEM images of the tire surface, captured after the initial and 20 cycles using an Apreo S microscope, reveal that discrete particles emerged in the friction area after 10 cycles, as illustrated in Figure 7.

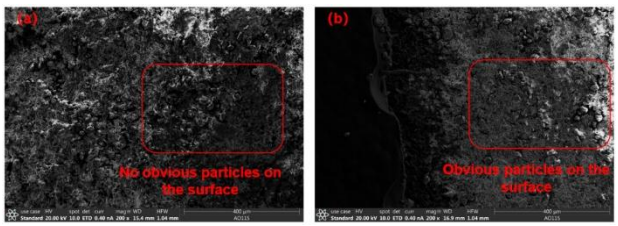

Figure 7. Surface morphology after cyclic loading observed under scanning electron microscopy: (a) Before cyclic loading; (b) After 10 cycles

To explore the impact of discrete particles on tire–asphalt friction, self-developed testing apparatus is employed in this work. The asphalt pavement is subjected to 20 cycles of friction, with loading paths of 0 mm-5 mm and 5 mm-0 mm. After reaching 20 cycles, the loading path is changed to 0 mm-10 mm and 10 mm-0 mm. In the new loading path, 0 mm-5 mm is the contact area at the beginning of the cycle friction, while 5 mm-10 mm and 10 mm-5 mm are the new friction areas. During this process, some of the abrasive particles generated by cyclic friction will be carried out. When the loading path becomes 5 mm-0 mm, it returns to the cyclic friction area, which is different from the initial path of 0 mm-5 mm. Compared with the initial state, some discrete particles in the cyclic friction region have been removed, and the loading path is illustrated in Figure 8(a). Figure 8(b) presents the friction force variation over time after 20 cycles, where the 0–5 mm segment remains within the cyclic region, and the 5–10 mm segment lies in the non-cyclic region, carrying the discrete particles generated by cyclic friction. Figure 8(c) shows the friction force variation along the 10–0 mm path, with the 10–5 mm segment in the non-cyclic region and the 5–0 mm segment entering the cyclic region. Comparing and analyzing the friction force variation curves of 0 mm -5 mm in Figure 8 (b) and 5 mm -0 mm in Figure 8 (c) above, it is found that the average friction force between the tire and asphalt pavement is significantly reduced, and the friction force curve is smoother. Based on the above discussion, when the discrete particles in the cyclic friction area are eliminated, the friction force curve tends to flatten and the friction force also significantly decreases. This also indicates that the discrete particles generated during the tire asphalt pavement cyclic friction process are one of the key factors for frictional instability.

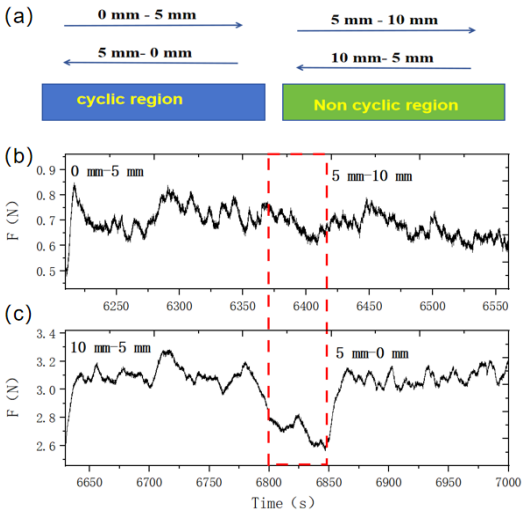

Figure 8. Time-varying frictional force curves across various intervals

4. THEORETICAL ANALYSIS

4.1. Impact of cyclic loading on tire surface roughness

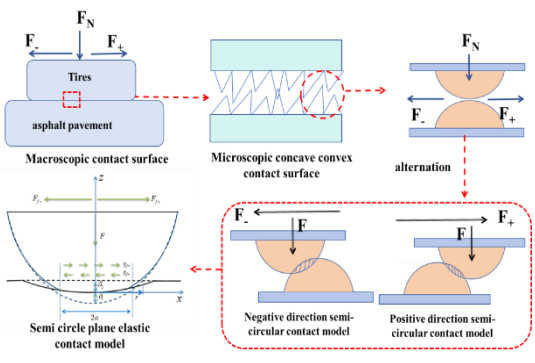

Figure 9. Semi-circular plane elastic contact model

At the macroscopic level, what appears to be a smooth interface between asphalt and tires is, in fact, a complex arrangement of numerous discrete and irregular microelements at the microscopic scale (Borgs et al., 1995; La et al., 2018; La, Wang, 2023).

Consequently, this study abstracts the intricate micro-concave-convex contact surface between asphalt and tires into an idealized semi-circular contact model. The cyclic friction phenomenon on asphalt pavements can be conceptualized as an alternation of contact and sliding between these semi-circular elements.

To facilitate computational analysis, the semi-circular contact is further simplified to a semi-circular plane contact model, which can be effectively analyzed using Hertzian contact theory. The model development process is illustrated in Figure 9.

When only the normal pressure F is considered in the model, the contact deformation between the hemisphere and the flat surface is illustrated in Figure 9, where δ_1 and δ_2 represent the displacements of the hemisphere and the flat surface, respectively. $2a$ denotes the length of the contact area, μ is Poisson's ratio, R is the radius of the hemisphere, r indicates the distance from the center along the X-axis, and E represents the elastic modulus.

For simplicity, the material properties of both the flat surface and the hemisphere are assumed to be identical, leading to the relation $\delta_1 = \delta_2$.

According to Hertzian contact theory, the contact radius, displacement, and stress distribution along the contact surface—specifically, the variation of stress distribution P_r and displacement δ —can be determined. Since the displacement of the hemisphere across the contact area essentially corresponds to the overlap between the hemisphere and the flat surface under normal pressure F , the total overlap can be obtained by integrating the displacement δ over the contact area.

When alternating tangential forces are applied, a uniformly distributed load is assumed within the overlapping region between the hemisphere and the flat surface, satisfying relation $F_{f+} = 2a \times q_{f+}$ Within the overlapping region $z = 0$, only the σ_x -component of stress is non-zero, and stress concentration occurs at the contact boundaries $x = a$、$x = -a$, as shown in Fig. 10.

Under alternating tangential stress, the maximum von Mises yield strength appears at the boundary of the hemisphere–flat overlap zone, accompanied by stress concentration. The yield strength gradually decreases with increasing distance from the contact interface.

Based on the above discussion, under cyclic friction on an asphalt pavement, when the tangential force acts in the positive direction, the left boundary of the overlapping region experiences tensile stress while the right boundary is subjected to compressive stress, resulting in stress concentration. Conversely, when the tangential force is reversed, the right boundary is under tension and the left boundary under compression, also leading to stress concentration.

Consequently, the overlapping region between the hemisphere and the flat surface undergoes alternating tensile and compressive stresses at its boundaries, causing fatigue shear damage within the overlapping zone.

The damaged material (i.e., the overlapping portion) becomes detached as discrete particles within the cyclic friction region and persists throughout the entire friction process.

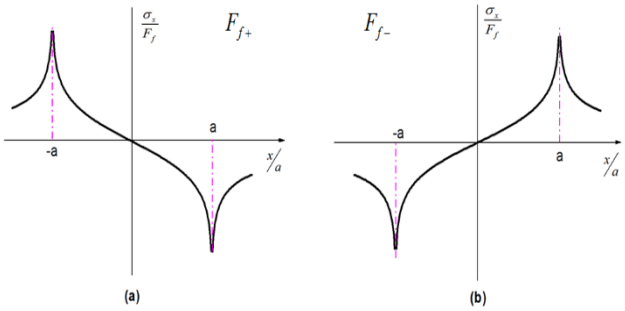

Figure 10. Tangential force-induced stress concentration: (a) Force along the positive X-axis; (b) Force along the negative X-axis.

To simulate the behavior of such microscopic asperities, the slider is discretized into $N \times N$ identical rigid blocks, with the mass of each block being the ratio of the total mass of the rubber slider to N^2 , while the concrete pavement is discretized into a rigid plane, as illustrated in Fig. 11.

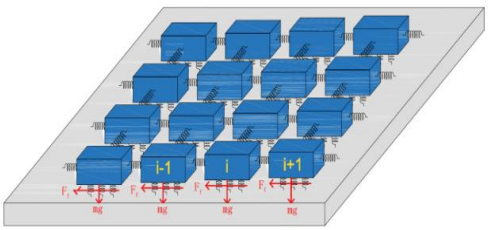

Figure 11. Spring-block model based on interfacial contact characteristics

The slider and the plane are connected by interfacial springs with a stiffness of $k_i = < k > (f_t / \overline{f_t})^2$, where $< k >$ represents the average equivalent stiffness of the interfacial connecting springs, and f_t denotes the strength of the interfacial springs.

Given the similarity between rough peaks and asperities, the strength distribution of the interfacial springs is described by a Gaussian distribution, with $\overline{f_t}$ being the average shear strength of the interfacial springs. Adjacent sliders are also

interconnected by springs, and the equivalent stiffness of a single slider is k_b, which is related to the elastic modulus of the rubber slider and the geometry of the segmentation.

The entire slider system is influenced solely by the external forces T_0 and T, with T_0 applied by the counterweight block to the first slider and T applied by the loading system to the Nth slider.

The system's stiffness and shear strength are primarily determined by the number of discrete sliders. By varying this number, the mechanical properties of the slider assembly are adjusted, and 100 sliders were used in the simulation.

A dynamic analysis is performed on the i-th block, which is subjected to forces from the adjacent left and right blocks, the interfacial frictional force, and its own gravitational force. The damping force and the interaction forces between blocks are formulated in an analogous manner. The horizontal dynamic behavior of the spring–block system along the interface is governed by:

$$M\ddot{u}(t) + C\dot{u}(t) + Ku(t) = Q(t) \quad (1)$$

with C representing the damping matrix, M the mass matrix, K the block stiffness matrix, and Q the external force applied to the system.

Results from the experiments reveal that repeated cyclic loading under alternating shear stress leads to a marked decrease in the material's surface roughness. Based on this observation, the computational model assumes that the elastic modulus and shear modulus of the material remain unchanged over 20 cycles, while the surface roughness is adjusted to simulate frictional characteristics under different cycling conditions.

As illustrated in Fig. 12, which shows the variation of friction force over time, subfigures (a) and (b) present the experimental and numerical results under the initial cycle, respectively. The comparison reveals qualitative agreement between experimental and numerical outcomes.

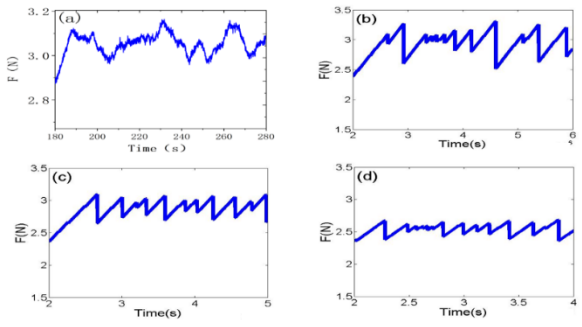

Figure 12. Variation curve of friction force with time under different cycle numbers: (a) experimental result during the initial cycle; (b) simulation result during the initial cycle; (c) simulation result after 10 cycles; (d) simulation result after 20 cycles

Subfigures (c) and (d) display the numerical simulation results after 10 and 20 cycles, demonstrating a gradual decrease in friction force and increasingly pronounced stick-slip phenomena with further cycling.

These trends are qualitatively consistent with experimental observations, thereby further validating the accuracy and reliability of the model.

5. CONCLUSION

(1) This study introduces a custom-designed testing apparatus to assess the cyclic friction performance of tire-asphalt pavement interactions. The apparatus has been rigorously calibrated to ensure its reliability and stability, meeting the strict requirements of experimental protocols.

(2) As the number of cycles increases, the tire surface roughness decreases, accompanied by the emergence of distinct discrete particles, which are identified as a key contributor to frictional instability. The underlying mechanism for the reduction in surface roughness under cyclic friction is explained using elastoplastic contact theory.

(3) The cyclic frictional behavior of asphalt pavement was numerically simulated using a spring-slider model, and the numerical results from the initial cycle qualitatively match the experimental findings; by adjusting the roughness parameter in the model, it was observed that the friction force gradually decreases and the stick-slip phenomenon diminishes with increasing number of cycles, which is consistent with the trends identified experimentally.

Acknowledgments

This work was supported by the Key Research and Development Projects of Qinghai Province (No. 2025-QY-229), awarded to the first author, La. The study is original, and all data and analyses presented in this paper were generated by the authors as part of their own research.

References

Adamcs, Piotrowski, M., 2012. Use of the unified theory of rubber friction for slip-resistance analysis in the testing of footwear outsoles and compounds. Footwear Sci., 4(1), pp. 23–35.

Beketov, A. and Khalimova, S., 2023. Impact of Roughness and Friction Properties of Road Surface of Urban Streets on the Traffic Safety. Komunikácie, 25(3), pp. 100–115.

Behrouz, M., Moghadas, F.N. and Hamzeh, Z., 2022. Automatic Pavement Texture Measurement Using a New 3D Image-Based Profiling System. Measurement, 199, p. 111234.

Borgs, C., De Coninck, J., Kotecký, R., et al., 1995. Does the roughness of the substrate enhance wetting? Phys. Rev. Lett., 74(12), p. 2292.

Chu, L., Cui, X., Zhang, K., et al., 2019. Directional skid resistance characteristics of road pavement: Implications for friction measurements by British pendulum tester and dynamic friction tester. Transp. Res. Rec., 2673(10), pp. 793–803.

Ciavarella, M., 2017. A simplified version of Persson's multiscale theory for rubber friction due to viscoelastic losses. J. Tribol., 140(1), pp. 1–20.

Fwa, T.F., 2017. Skid resistance determination for pavement management and wet-weather road safety. Int. J. Transp. Sci. Technol., 6(3), pp. 217–227.

Georgouli, K., Plati, C. and Loizos, A., 2016. Assessment of dynamic modulus prediction models in fatigue cracking estimation. Mater. Struct., 49(12), pp. 5007–5019.

Gerardo, W., Flintsch, et al., 2018. Evaluation of International Friction Index Coefficients for Various Devices. Transp. Res. Rec., 2094(1), pp. 136–143.

Guo, K., 2016. UniTire: 统一轮胎模型 (UniTire: Unified Tire Model). Chin. J. Mech. Eng., 52(12), pp. 90–99.

Gupta, A., Pradhan, S.K., et al., 2020. Numerical analysis of rubber tire/rail contact behavior in road cum rail vehicle under different inflation pressure values using finite element method. Mater. Today: Proc., 47, pp. 6628–6635.

He, Y., Yang, X., Xiao, S., et al., 2023. Experimental study on the high-speed frictional behavior between the tire and asphalt pavement. Constr. Build. Mater., 371, p. 130782.

Hofko, B., Kugler, H., Chankov, G., et al., 2019. A laboratory procedure for predicting skid and polishing resistance of road surfaces. Int. J. Pavement Eng., 20(4), pp. 439–447.

Juan, C.A., 2017. Optimization of an optical test bench for tire properties measurement and tread defects characterization. Sensors, 17(4), pp. 707–713.

Kane, M. and Edmondson, V., 2022. Tire/road friction prediction: Introduction of a simplified numerical tool based on contact modeling. Veh. Syst. Dyn., 60(3), pp. 770–789.

Krishnanunni, C. and Rao, B., 2019. Decoupled technique for dynamic response of vehicle-pavement systems. Eng. Struct., 191, pp. 264–279.

La, S., Wang, J., Zhang, X., et al., 2018. Frictional behavior of a micro-sized superconducting fiber in a low-temperature medium: Experimental and computational analysis. Acta Mech. Solida Sin., 31, pp. 405–415.

La, S. and Wang, C., 2023. Experimental and numerical calculation of the friction performance of a concrete surface. Materials, 16(8), p. 2989.

Lin, C. and Tongjing, W., 2018. Effect of fine aggregate angularity on skid-resistance of asphalt pavement using accelerated pavement testing. Constr. Build. Mater., 168, pp. 41–46.

Liu, Y., Xu, X., Huang, Z., et al., 2023. Discrete-Continuous Coupling Simulation and Analysis for Asphalt Pavement Dynamic Stress Responses under a Moving Wheel Load. Case Stud. Constr. Mater., 1818(1), pp. 214–245.

Liu, Z., Wang, F., Cai, Z., et al., 2023. A novel theoretical model of tire in-plane dynamics on uneven roads and its experimental validation. Mech. Syst. Signal Process., 186, p. 109854.

Luo, L., Yang, S.-H., Oeser, M. and Liu, P., 2024. Moisture damage mechanism of asphalt mixtures containing reclaimed asphalt pavement binder: A novel molecular dynamics study. J. Clean. Prod., 475, p. 143711.

Mahajan, G.R., Radhika, B. and Biligiri, K.P., 2022. A critical review of vehicle-pavement interaction mechanism in evaluating flexible pavement performance characteristics. Road Mater. Pavement Des., 23(4), pp. 735-769.

Novikov, I. and Lazarev, D., 2017. Experimental Installation for Calculation of Road Adhesion Coefficient of Locked Car Wheel. Transp. Res. Procedia, 20, pp. 463–467.

Qian, Z. and Meng, L., 2017. Study on micro-texture and skid resistance of aggregate during polishing. Front. Struct. Civ. Eng., 11, pp. 346–352.

Rith, M., Kim, K.Y. and Lee, W.S., 2020. Characterization of long-term skid resistance in exposed aggregate concrete pavement. Constr. Build. Mater., 256, p. 119390.

Roy, U., Farid, A. and Ksaibati, K., 2023. Effects of pavement friction and geometry on traffic crash frequencies: A case study in Wyoming. Int. J. Pavement Res. Technol., 16(06), pp. 1468–1481.

Sajid, H.U., Naik, D.L. and Kiran, R., 2021. Improving the ice-melting capacity of traditional deicers. Constr. Build. Mater., 271, p. 121527.

Sara, A., Ahmadreza, M., Amir, G., et al., 2021. Automatic pavement rutting measurement by fusing a high speed-shot camera and a linear laser. Constr. Build. Mater., 283, p. 122682.

Serigos, P., Andre, D. and Prozzi, J., 2016. Incorporating surface microtexture in the prediction of skid resistance of flexible pavements. Transp. Res. Rec., 2457, pp. 105–113.

Tan, T., Xing, C., Tan, Y., et al., 2019. Safety aspects on icy asphalt pavement in cold region through field investigations. Cold Reg. Sci. Technol., 161, pp. 21–31.

Tomaraee, P., Mardani, A., Mohebbi, A., et al., 2015. Relationships among the contact patch length and width, the tire deflection, and the rolling resistance of a free-running wheel in a soil bin facility. Span. J. Agric. Res., 13(2), p. 0211.

Wang, W., Yan, S. and Zhao, Y., 2015. Numerical and experimental studies of a radial truck tire with tread pattern. Simul., 91(11), pp. 970–979.

Wei, H., Zhang, H., Li, J., et al., 2023. Effect of loading rate on failure characteristics of asphalt mixtures using acoustic emission technique. Constr. Build. Mater., 364, p. 129835.

Yan, B., Mao, H., Zhong, S., Zhang, P. and Zhang, A., 2019. Experimental study on wet skid resistance of asphalt pavements in icy conditions. Materials, 12(8), p. 1201.

Yu, M., You, Z., Wu, G., et al., 2020. Measurement and modeling of skid resistance of asphalt pavement: A review. Constr. Build. Mater., 260, p. 119878.